

Resolving Geometric Excitations of Fractional Quantum Hall States

Yang Liu,^{1,2} Tongzhou Zhao,¹ and T. Xiang^{1,2,*}

¹*Beijing National Laboratory for Condensed Matter Physics and Institute of Physics,
Chinese Academy of Sciences, Beijing 100190, China.*

²*School of Physical Sciences, University of Chinese Academy of Sciences, Beijing 100049, China.*

The quantum dynamics of the intrinsic metric profoundly influence the neutral excitations in the fractional quantum Hall system, as established by Haldane in 2011 [1], and further evidenced by a recent two-photon experiment [2]. Despite these advancements, a comprehensive understanding of the dynamic properties of these excitations, especially at long wavelengths, continues to elude interest. In this study, we employ tensor-network methods to investigate the neutral excitations of the Laughlin and Moore-Read states on an infinite cylinder. This investigation deepens our understanding of the excitation spectrum in regions where traditional methods do not work effectively. The spectral functions for both states reveal the presence of $S = -2$ geometric excitations. For the first time, we unveil the complex spectra of both neutral fermion and bosonic Girvin-MacDonald-Platzman modes within the excitation continuum by calculating the three-particle density response function for the Moore-Read state. Our findings support the hypothesis of emergent supersymmetry and highlight the potential for detecting neutral fermions in future experiments.

Introduction — Neutral excitations in the fractional quantum Hall effect (FQHE) have drawn intensive attention over the past decades. The pioneering work by Girvin, MacDonald and Platzman [3, 4] interprets the neutral excitation in the Laughlin state [5] as a collective density fluctuation mode, called the magnetoroton, analogous to the roton excitation in superfluid helium [6–9]. The lowest neutral excitation was later identified as a composite fermion exciton mode [10–14]. Haldane proposed a geometric interpretation of this mode in the long-wavelength limit, suggesting that the fluctuation of the intrinsic metric determines its dynamics [1, 15, 16]. More specifically, perturbations on the metric introduce a new excitation in the d-wave channel, possessing both chirality and topological order [17–27], which was observed by circularly polarized resonant inelastic light scattering [2].

The Moore-Read (MR) state [28–30] involves the pairing of composite fermions [31], resulting in two types of excitations depending on the electron number: a magnetoroton appears when the electron number is even (even parity), while a neutral fermion emerges when the electron number is odd (odd parity), confirmed by the exact diagonalization [32–34]. Unlike the magnetoroton, a neutral fermion carries a half-integer angular momentum [35]. The edge states corresponding to the neutral fermions possess non-Abelian statistics. Through quantum interference, they have great potential in the application of topological quantum computing [36–39].

Recent studies indicate that both types of excitations can be integrated into a cohesive theory if identified as superpartners of an emergent supersymmetry [40] that can be detected from its bulk or edge excitations [41, 42]. For the MR state, the two bulk excitations correspond to two edge states known as the chiral charge boson and the copropagating Majorana fermion, associated with $\mathcal{N} = (1, 0)$ supersymmetry in $(1+1)$ dimensions [43, 44]. According to this theory, these excitations should merge

in the long-wavelength limit as a manifestation of supersymmetry. However, due to finite size constraints, achieving this limit is challenging with exact diagonalization or other numerical methods.

In this study, we calculate the dynamical spectral functions of the FQHE states on an infinite cylinder using the matrix product state (MPS) renormalization group under the single-mode approximation [45]. Our results demonstrate that MPS can accurately capture the bosonic magnetoroton and neutral fermion excitations in the continuum, providing more detailed information than the existing theory. Moreover, we find that the neutral magnetoroton mode in the long-wavelength limit is a $S = -2$ geometric excitation (also called a graviton in the literature [46–51]).

Model and method — Let us consider a two-dimensional electron gas confined to the lowest Landau level on an infinite cylinder along the x-axis with circumference L_y . The parent Hamiltonian of the Laughlin state in the Landau gauge is defined by a two-body interaction

$$H_L = \sum_k V_k \rho_k \rho_{-k}, \quad (1)$$

where V_k is the Fourier transform of a projected pseudopotential [52, 53]. $k = (k_x, k_y)$ is the momentum of electron with $k_y = ne_y$ (n an integer) and $e_y = 2\pi/L_y$. k_x is continuous on an infinite cylinder. ρ_k is the projected density operator defined in terms of the electron operator c_n in the orbital basis space as

$$\rho_{\tilde{k}_x, me_y} = \sum_n e^{i\tilde{k}_x(2n+m)/2} c_n^\dagger c_{n+m}, \quad (2)$$

where $\tilde{k}_x = k_x e_y$.

Similarly, the parent Hamiltonian of the MR state is defined by a three-body interaction [35]:

$$H_{MR} = \sum_{k_1 k_2} V_{k_1 k_2} \rho_{k_1} \rho_{k_2} \rho_{-k_1 - k_2} \quad (3)$$

where V_{k_1, k_2} is the Fourier transform of a three-body interaction [35]. Detailed derivations of Eqs. (1) and (3) are given in Supplemental Material (SM) [54].

We construct the MPS representation of FQHE states using variational optimization instead of the conventional conformal field theory approach [55–57]. It is noteworthy that the ground states are derived from different orbital configurations [58, 59]. For example, in the 1/3-filling Laughlin state, the ground states are triply degenerate, corresponding to the initial orbital configurations of $\{\dots 100100\dots\}$, $\{\dots 010010\dots\}$ and $\{\dots 001001\dots\}$, respectively. These configurations are translationally invariant with a periodicity of three, effectively acting as a unit cell for these states. Similarly, ground states in other FQHE systems also demonstrate translational invariance, albeit with the same or different unit cell sizes. Thus, the ground state of FQHE can be effectively modeled by a translationally invariant MPS:

$$\Psi = \dots \text{---} \textcircled{A} \text{---} \textcircled{A} \text{---} \textcircled{A} \text{---} \dots, \quad (4)$$

where A is a local tensor defined for each unit cell. If a unit cell contains M sites, we can further decompose A as a product of M local tensors defined by A_l ($l = 1, \dots, M$)

$$\textcircled{A} = \textcircled{A_1} \textcircled{A_2} \dots \textcircled{A_M}. \quad (5)$$

For the above Laughlin state, $M = 3$. For the MR state at $\nu = 1/2$ filling, the minimal orbital configuration to achieve a ground state of even parity is $\{\dots 10011001\dots\}$, allowing us to use $M = 4$.

However, MR is a system of pairing composite fermions in analogy to a p-wave superconductor. The neutral fermion only occurs in the system with an odd number of fermions, so we take half of the cell of pairing fermions as an unpaired ground state: $\{\dots 01\dots\}$ is the unpaired configuration of $\{\dots 1001\dots\}$ that contains one fermion excitation. Thus, in the study of neutral fermions, we can reduce the unit cell size from $M = 4$ to $M = 2$.

The vertical leg of A_i represents the local physical degrees of freedom with quantum numbers (K_i, C_i) , where C_i denotes the electron number and K_i equals the orbital momentum \hat{K}_i . If the MR state in the odd parity sector with a unit cell $M = 2$ is studied, we should attach a one-half quantum flux $f = 1/2$ to the first local tensor in each unit cell. This additional flux modifies the momentum \hat{K}_i at that site to $K_i = \hat{K}_i + f$.

Similarly, the two horizontal legs also carry quantum numbers, denoted as (\bar{K}_i, \bar{C}_i) . The quantum numbers on the three legs of the same tensor must satisfy the rule:

$$(\bar{K}, \bar{C})_{i, \text{left}} + (K_i, C_i) - (\bar{K}, \bar{C})_{i, \text{right}} = 0 \quad (6)$$

The projected guiding center structure factor, defined by the following static density-density correlation func-

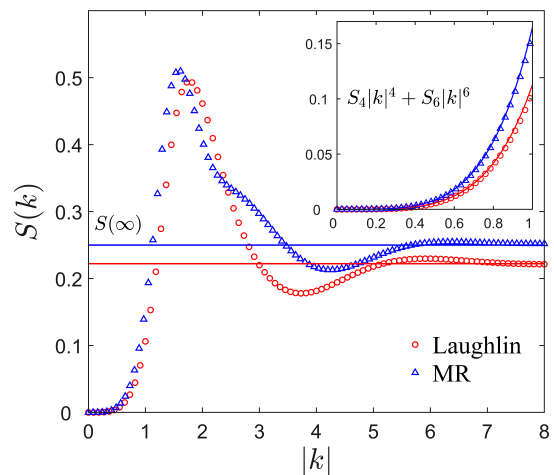


FIG. 1. Static structure factor $S(k)$ for the Laughlin and MR states along the momentum line $k = (k_x, 0)$. The solid lines are theoretical predictions $S(k \rightarrow \infty) = \nu(1 - \nu)$ with ν the filling factor [16]. The inset shows the structure factor in the long-wavelength limit. The solid curves are the field theory results with $S_4 = \nu s/4$ and $S_6 = \nu s[s - (c - \nu)/(12\nu s)]/8$, s the guiding center spin and c the central charge [47, 61–67].

tion, characterizes the incompressibility of FQHE:

$$S(k) = \frac{1}{N} \langle \delta\rho_k \delta\rho_{-k} \rangle, \quad (7)$$

where $\delta\rho_k = \rho_k - \langle \rho_k \rangle$ is the fluctuation of the density operator. Figure 1 shows the MPS results for the structure factors in the Laughlin and MR states (details are presented in SM). It indicates that both states are incompressible fluids, although their corresponding MPS representations are periodic in unit cells. In the long-wavelength limit, $S(k)$ could be expanded as

$$S(k) = S_2|k|^2 + S_4|k|^4 + S_6|k|^6 + \dots \quad (8)$$

In a topologically gapped system, one has $S_2 = 0$ and the leading contribution is from the S_4 term [60].

Under the single-mode approximation, the excited states are represented by a momentum-boosted MPS in the tangent space of Ψ [68–71]

$$\Phi_k(B) = \sum_n e^{i\bar{k}_x n M} \dots \textcircled{A} \textcircled{B} \textcircled{A} \dots, \quad (9)$$

where B is an impurity tensor defined on the n th unit cell. In a unit cell of M sites, B is a sum of M MPS, where A_i in the i th MPS ($i = 1, \dots, M$) is substituted by a local impurity tensor B_i multiplied by a site-dependent phase factor. For example, for a $M = 2$ system, B is defined as

$$\textcircled{B} = \textcircled{B_1} \textcircled{A_2} + e^{i\bar{k}_x} \textcircled{A_1} \textcircled{B_2}. \quad (10)$$

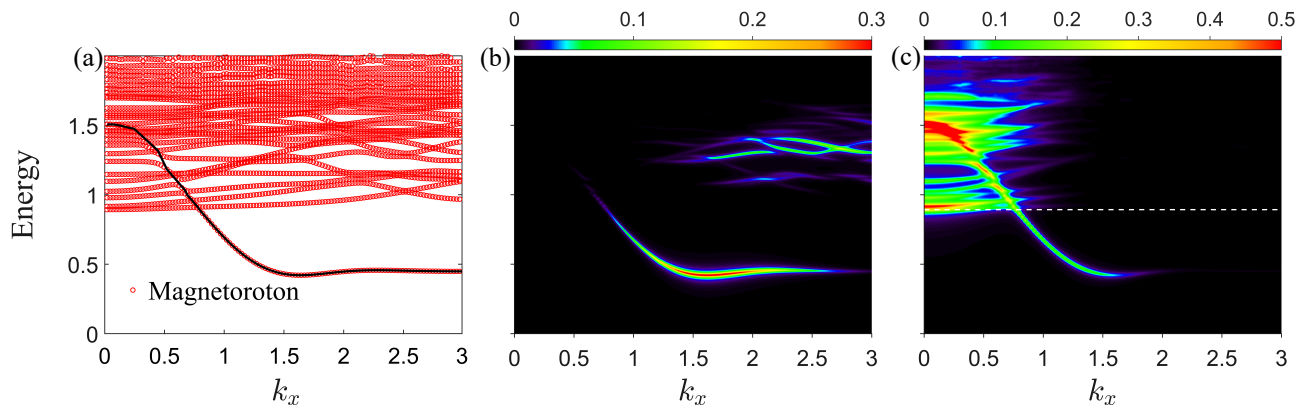


FIG. 2. (a) Energy dispersions of the excited states for the $\nu = 1/3$ Laughlin state on an infinite cylinder with $L_y = 18$ along the momentum line $k = (k_x, 0)$, obtained with an MPS bond dimension $D = 88$. (b) Single-particle density spectra. (c) Pairing density spectra of O^- . The white dashed line represents the lower bound of the continuum. The black line in (a) sketches the energy dispersion of the magnetoroton with the highest spectral weight at $(k = 0, E = 1.5)$ in (c).

Spectral functions — Upon determining all the local tensors variationally, we can use the eigenvalues and eigenfunctions of the ground and excited states to evaluate the spectral function of a physical variable O_k

$$I(\omega, k) = \sum_n |\langle \Phi_{k,n}(B) | O_k | \Psi(A) \rangle|^2 \delta(\hbar\omega - E_n), \quad (11)$$

where E_n is the n th eigenvalue of the excited state and $\Phi_{k,n}$ the corresponding eigenfunction.

In the $\nu = 1/3$ Laughlin state, the lowest collective excitations are the bosonic magnetoroton modes. This mode essentially represents a quantized wave of charge density propagating through the electron system, detectable by the single-particle density spectral function of $O_k = \delta\rho_k$. As shown in Fig. 2(a-b), the dispersion of this mode becomes flat in the large k limit, indicating that it is a composite fermion exciton mode as predicted by Scarola *et. al* [10]. The spectrum shows a distinct magnetoroton minimum at $k \approx 1.7$ with an energy $E = 0.41$, indicating a softening of this mode at a specific length scale. At small k , the magnetoroton mode merges into the continuum of excitations, and its spectral weight diminishes significantly, primarily due to the quartic dependence of $S(k)$ on k .

The single-particle density spectrum also reveals pronounced features of charge-neutral excitations, known as excitons, in the high-energy continuum, with momentum k ranging from 2 to 3 and energy E from 1.25 to 1.4. These features likely arise from the excitation of composite fermions to higher effective Landau levels in the composite fermion theory [72–75]. This finding aligns with earlier calculations [76] and is consistent with inelastic photon measurement results [77].

In this Laughlin state, the intrinsic metric associated with magnetoroton couples directly with the two-particle density operators in the long wavelength limit. Thus, to reveal the magnetoroton mode in the continuum, we cal-

culate the pair density spectrum Eq. (11) with O_k defined by

$$O_k^\pm = \sum_{k_1+k_2=k} k_1^\pm k_2^\pm e^{-(k_1^2+k_2^2)/4} \delta\rho_{k_1} \delta\rho_{k_2}, \quad (12)$$

where $k^\pm = k_x \pm ik_y$, corresponding to the $S = 2$ and $S = -2$ representations, respectively. We also evaluate the dynamical spectra of other d-wave operators $O_{x^2-y^2} = O^+ + O^-$ and $O_{xy} = O^+ - O^-$. The calculation reveals that only the $S = -2$ mode contributes to the long-wavelength magnetoroton spectra in the continuum. More specifically, the $S = -2$ spectrum shows a strong signal at $k = 0$ and $E \approx 1.5$, as depicted in Fig. 2(c), consistent with the exact diagonalization results [22].

At $k = 0$, the $S = -2$ spectrum also reveals a peak just above the lower edge of the continuum at $E = 0.9$. This peak corresponds to a bi-roton bound state, where two rotons interact by dipole-dipole interaction to form a bound state with an energy lower than the magnetoroton mode in the continuum [78–80]. However, this bound state does not possess the chirality characteristic of the geometric, aligning with recent experimental results [2].

Next, we turn to the excitations of the MR state. In the MR state, electrons pair up in a p-wave superconducting-like manner. In addition to the magnetoroton modes, neutral fermion modes emerge in this state. These modes can be described by Majorana fermions bound to vortex excitations in the p-wave paired state.

Based on the calculations of single and three-particle density spectra, we identify two types of excitations, as shown in Fig. 3(a-b). The first type is the bosonic magnetoroton modes, which exhibit energy dispersions similar to those in the Laughlin states. The second type is the neutral fermion modes, which features a distinct local minimum at $k_x = 1$. Our results are consistent with previous finite-system calculations based on the bipartite

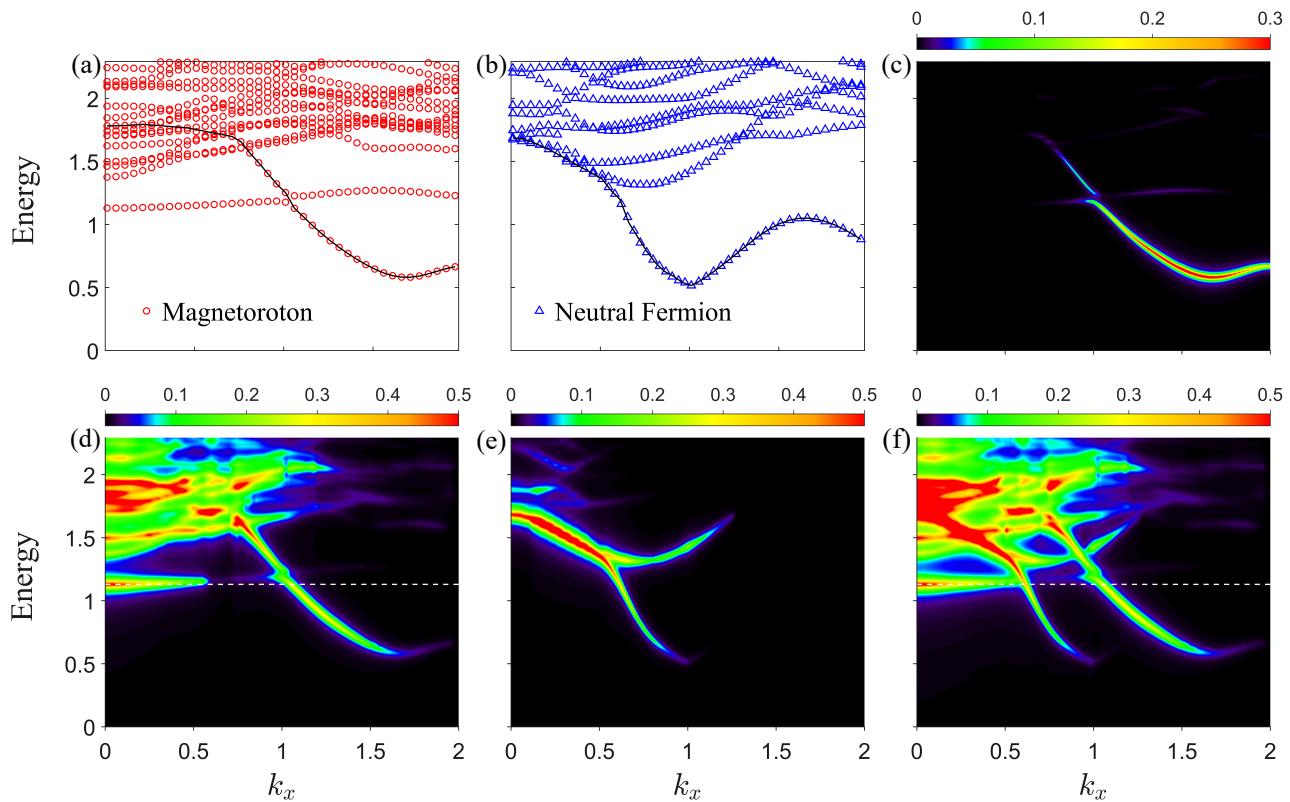


FIG. 3. Spectral functions of the $\nu = 1/2$ MR state on an infinite cylinder with $L_y = 16$, obtained along the momentum points $k = (k_x, 0)$ with $D = 103$. Energy dispersions of the excited states in (a) the even- and (b) odd-parity sectors. (c) Single particle density spectra. (d-e) Three-particle density spectra of O^- in the even- and odd-parity sectors, respectively. (f) Combined three-particle density spectra of (d) and (e). The black curve in (a) is a guiding line that traces the high-intensity points in the small k region with the magnetoroton mode shown in (c) and (d). The black curve in (b) is the energy dispersion of the lowest excited states in the odd-parity MR state. The thin white dashed lines in (d) and (f) are the lower edge of the continuum.

composite fermions, Jack Polynomials, symmetrization constructions on multilayer systems, and supersymmetric wave functions [81–84].

The single-particle density spectrum, depicted in Fig. 3(c), shows similar results to those in the Laughlin state (see Fig. 2(a)). Notably, the low-energy magnetoroton excitation exhibits a prominent peak at $k_x \approx 1.6$ and $E = 0.57$. However, the spectrum becomes heavily damped upon entering the two-particle excitation continuum. Like the Laughlin state, it shows no spectral weight for the magnetoroton modes in the long-wavelength limit.

Unlike in the Laughlin state, the magnetoroton mode does not display a sizable weight in the pair density spectra in the long-wavelength limit due to the paired nature of electrons in the MR state. This pairing modifies the geometry and metric that govern the interactions and correlations. Consequently, the magnetoroton modes do not impact the MR state similarly to the Laughlin state, especially in the pair density channel.

However, the magnetoroton modes respond strongly to the dynamic fluctuation of the three-particle density

operator

$$O_k^\pm = \sum_{k_1 k_2 k_3} k_1^\pm (k_2^\pm + k_3^\pm) e^{-(k_1^2 + k_2^2 + k_3^2)/4} \delta \rho_{k_1} \delta \rho_{k_2} \delta \rho_{k_3} \delta_{k_1 + k_2 + k_3, k}. \quad (13)$$

Again, O^\pm corresponds to the $S = \pm 2$ state. Figure 3(d) illustrates the magnetoroton spectra acquired in the O^- channel. Similar to the Laughlin state, there is a distinct magnetoroton response in the small k region within the continuum. Compared to the $S = -2$ mode of the Laughlin state, the spectrum of this mode in the MR state is more broadened in the low- k region, consistent with the result presented in Ref. [22].

Magnetoroton modes are linked to collective density oscillations, whereas neutral fermion modes are closely associated with the topological excitations of the MR state. To explore the neutral fermion modes, we compute the MR ground state and the corresponding excited states in the odd parity sector. The analysis of response functions reveals that both the pair and three-particle density spectral functions exhibit distinct peaks of neutral fermions. Figure 3(e) shows the three-particle den-

sity spectra in the neutral fermion channel. This is the first time the spectral function of neutral fermions in the small k limit is obtained. As illustrated by Fig. 3(f), the magnetoroton and neutral fermion modes tend to merge at $k = 0$, hinting at an underlying emergent supersymmetry. Furthermore, the energy of the magnetoroton mode is higher than that of the neutral fermion mode in the continuum, consistent with the published result for the two modes obtained by parametrizing the superspace [84].

Conclusion and discussion— In summary, we investigate the neutral excitations of the $\nu = 1/3$ Laughlin state and the $\nu = 1/2$ MR state under the single-mode approximation of MPS on an infinite cylinder. Our analysis of the Laughlin state pinpoints the magnetoroton minimum and elucidates the long-wavelength magnetoroton mode within the continuum through the pair density spectral function. From the long-wavelength spectra, we confirm that the magnetoroton mode corresponds to the $S = -2$ geometric excitation.

For the MR state, we have developed the MPS representations for both ground and excited states across even and odd parity sectors. We probe the bosonic magnetoroton and neutral fermion modes in the MR state in the small k region, inaccessible via exact diagonalization due to the finite-size effects. Our results confirm that these modes are consistent with the previously proposed emergent supersymmetry. It is worth exploring whether incorporating supersymmetry into effective field theory might pair these two modes as superpartners [47]. The dynamic spectra we obtain will also contribute to constructing corresponding massive wave equations for these fields.

Our calculation is based on the parent Hamiltonians, which account only for short-range interactions, not the long-range Coulomb interaction. Nevertheless, we believe that our findings still offer significant qualitative insights into the physics underlying FQHE. Our results suggest that the neutral fermion mode might be explored experimentally through multi-photon experiments, providing a new avenue for empirical verification.

Acknowledgments— We have implemented the code for the excited spectrum based on ITensor [85]. We thank Songyang Pu, Zlatko Papić, Kun Yang, Ying Hai Wu, Tong Liu, Lingjie Du, Ajit C. Balram and J. K. Jain for helpful discussions. We thank J. Haegeman for the instructions on the KrylovKit package. This work is supported by the NSFC grant No. 12488201, and by the China Postdoctoral Science Foundation grant No. 2023M743742.

* txiang@iphy.ac.cn

[1] F. D. M. Haldane, Geometrical description of the frac-

tional quantum hall effect, *Phys. Rev. Lett.* **107**, 116801 (2011).

- [2] J. Liang, Z. Liu, Z. Yang, Y. Huang, U. Wurstbauer, C. R. Dean, K. W. West, L. N. Pfeiffer, L. Du, and A. Pinczuk, Evidence for chiral graviton modes in fractional quantum hall liquids, *Nature*, 1 (2024).
- [3] S. M. Girvin, A. H. MacDonald, and P. M. Platzman, Collective-excitation gap in the fractional quantum hall effect, *Phys. Rev. Lett.* **54**, 581 (1985).
- [4] S. M. Girvin, A. H. MacDonald, and P. M. Platzman, Magneto-roton theory of collective excitations in the fractional quantum hall effect, *Phys. Rev. B* **33**, 2481 (1986).
- [5] R. B. Laughlin, Anomalous quantum hall effect: An incompressible quantum fluid with fractionally charged excitations, *Phys. Rev. Lett.* **50**, 1395 (1983).
- [6] A. Bijl, J. De Boer, and A. Michels, Properties of liquid helium ii, *Physica* **8**, 655 (1941).
- [7] R. P. Feynman, Atomic theory of the λ transition in helium, *Phys. Rev.* **91**, 1291 (1953).
- [8] R. P. Feynman, Atomic theory of the two-fluid model of liquid helium, *Phys. Rev.* **94**, 262 (1954).
- [9] R. P. Feynman and M. Cohen, Energy spectrum of the excitations in liquid helium, *Phys. Rev.* **102**, 1189 (1956).
- [10] V. W. Scarola, K. Park, and J. K. Jain, Rotons of composite fermions: Comparison between theory and experiment, *Phys. Rev. B* **61**, 13064 (2000).
- [11] R. R. Du, H. L. Stormer, D. C. Tsui, L. N. Pfeiffer, and K. W. West, Experimental evidence for new particles in the fractional quantum Hall effect, *Phys. Rev. Lett.* **70**, 2944 (1993).
- [12] A. Pinczuk, B. S. Dennis, L. N. Pfeiffer, and K. West, Observation of collective excitations in the fractional quantum hall effect, *Phys. Rev. Lett.* **70**, 3983 (1993).
- [13] M. Kang, A. Pinczuk, B. S. Dennis, L. N. Pfeiffer, and K. W. West, Observation of multiple magnetorotons in the fractional quantum hall effect, *Phys. Rev. Lett.* **86**, 2637 (2001).
- [14] I. V. Kukushkin, J. H. Smet, V. W. Scarola, V. Umansky, and K. von Klitzing, Dispersion of the excitations of fractional quantum hall states, *Science* **324**, 1044 (2009), <https://www.science.org/doi/pdf/10.1126/science.1171472>.
- [15] F. D. M. Haldane, (2009), arXiv:0906.1854 [cond-mat.str-el].
- [16] F. D. M. Haldane, (2011), arXiv:1112.0990 [cond-mat.str-el].
- [17] R.-Z. Qiu, F. D. M. Haldane, X. Wan, K. Yang, and S. Yi, Model anisotropic quantum hall states, *Phys. Rev. B* **85**, 115308 (2012).
- [18] B. Yang, Z. Papić, E. H. Rezayi, R. N. Bhatt, and F. D. M. Haldane, Band mass anisotropy and the intrinsic metric of fractional quantum hall systems, *Phys. Rev. B* **85**, 165318 (2012).
- [19] K. Yang, Acoustic wave absorption as a probe of dynamical geometrical response of fractional quantum hall liquids, *Phys. Rev. B* **93**, 161302 (2016).
- [20] B. Yang, Z.-X. Hu, C. H. Lee, and Z. Papić, Generalized pseudopotentials for the anisotropic fractional quantum hall effect, *Phys. Rev. Lett.* **118**, 146403 (2017).
- [21] Z. Liu, A. Gromov, and Z. Papić, Geometric quench and nonequilibrium dynamics of fractional quantum hall states, *Phys. Rev. B* **98**, 155140 (2018).
- [22] S.-F. Liou, F. D. M. Haldane, K. Yang, and E. H. Rezayi, Chiral gravitons in fractional quantum hall liquids, *Phys. Rev. Lett.* **123**, 146801 (2019).

- [23] K. Yang, M. O. Goerbig, and B. Douçot, Collective excitations of quantum hall states under tilted magnetic field, *Phys. Rev. B* **102**, 045145 (2020).
- [24] Z. Liu, A. C. Balram, Z. Papić, and A. Gromov, Quench dynamics of collective modes in fractional quantum hall bilayers, *Phys. Rev. Lett.* **126**, 076604 (2021).
- [25] D. X. Nguyen and D. T. Son, Probing the spin structure of the fractional quantum hall magnetoroton with polarized raman scattering, *Phys. Rev. Res.* **3**, 023040 (2021).
- [26] D. X. Nguyen, F. D. M. Haldane, E. H. Rezayi, D. T. Son, and K. Yang, Multiple magnetorotons and spectral sum rules in fractional quantum hall systems, *Phys. Rev. Lett.* **128**, 246402 (2022).
- [27] C. Han and Z. Liu, Anisotropy and quench dynamics of quasiholes in fractional quantum hall liquids, *Phys. Rev. B* **105**, 045108 (2022).
- [28] G. Moore and N. Read, Nonabelions in the fractional quantum hall effect, *Nuclear Physics B* **360**, 362 (1991).
- [29] N. Read and E. Rezayi, Beyond paired quantum hall states: Parafermions and incompressible states in the first excited landau level, *Phys. Rev. B* **59**, 8084 (1999).
- [30] N. Read and D. Green, Paired states of fermions in two dimensions with breaking of parity and time-reversal symmetries and the fractional quantum hall effect, *Phys. Rev. B* **61**, 10267 (2000).
- [31] J. K. Jain, Composite-fermion approach for the fractional quantum hall effect, *Phys. Rev. Lett.* **63**, 199 (1989).
- [32] G. Möller, A. Wójs, and N. R. Cooper, Neutral fermion excitations in the moore-read state at filling factor $\nu = 5/2$, *Phys. Rev. Lett.* **107**, 036803 (2011).
- [33] P. Bonderson, A. E. Feiguin, and C. Nayak, Numerical calculation of the neutral fermion gap at the $\nu = 5/2$ fractional quantum hall state, *Phys. Rev. Lett.* **106**, 186802 (2011).
- [34] Z. Papić, F. D. M. Haldane, and E. H. Rezayi, Quantum phase transitions and the $\nu=5/2$ fractional hall state in wide quantum wells, *Phys. Rev. Lett.* **109**, 266806 (2012).
- [35] M. Greiter, X.-G. Wen, and F. Wilczek, Paired hall state at half filling, *Phys. Rev. Lett.* **66**, 3205 (1991).
- [36] P. Bonderson, Splitting the topological degeneracy of non-abelian anyons, *Phys. Rev. Lett.* **103**, 110403 (2009).
- [37] W. Bishara and C. Nayak, Odd-even crossover in a non-abelian $\nu = 5/2$ interferometer, *Phys. Rev. B* **80**, 155304 (2009).
- [38] W. Bishara, P. Bonderson, C. Nayak, K. Shtengel, and J. K. Slingerland, Interferometric signature of non-abelian anyons, *Phys. Rev. B* **80**, 155303 (2009).
- [39] B. Rosenow, B. I. Halperin, S. H. Simon, and A. Stern, Exact solution for bulk-edge coupling in the non-abelian $\nu = 5/2$ quantum hall interferometer, *Phys. Rev. B* **80**, 155305 (2009).
- [40] A. Gromov, E. J. Martinec, and S. Ryu, Collective excitations at filling factor $5/2$: The view from superspace, *Phys. Rev. Lett.* **125**, 077601 (2020).
- [41] K. K. W. Ma, R. Wang, and K. Yang, Realization of supersymmetry and its spontaneous breaking in quantum hall edges, *Phys. Rev. Lett.* **126**, 206801 (2021).
- [42] P. Salgado-Rebolledo and G. Palumbo, Nonrelativistic supergeometry in the moore-read fractional quantum hall state, *Phys. Rev. D* **106**, 065020 (2022).
- [43] C. Hull and E. Witten, Supersymmetric sigma models and the heterotic string, *Physics Letters B* **160**, 398 (1985).
- [44] S. Gates Jr, M. T. Grisaru, L. Mezincescu, and P. Townsend, (1, 0) supergravity, *Nuclear Physics B* **286**, 1 (1987).
- [45] R. Chi, Y. Liu, Y. Wan, H.-J. Liao, and T. Xiang, Spin excitation spectra of anisotropic spin-1/2 triangular lattice heisenberg antiferromagnets, *Phys. Rev. Lett.* **129**, 227201 (2022).
- [46] S. Golkar, D. X. Nguyen, and D. T. Son, Spectral sum rules and magneto-roton as emergent graviton in fractional quantum hall effect, *Journal of High Energy Physics* **2016**, 10.1007/jhep01(2016)021 (2016).
- [47] A. Gromov and D. T. Son, Bimetric theory of fractional quantum hall states, *Phys. Rev. X* **7**, 041032 (2017).
- [48] F. D. M. Haldane, E. H. Rezayi, and K. Yang, Graviton chirality and topological order in the half-filled landau level, *Phys. Rev. B* **104**, L121106 (2021).
- [49] A. Kirmani, K. Bull, C.-Y. Hou, V. Saravanan, S. M. Saeed, Z. Papić, A. Rahmani, and P. Ghaemi, Probing geometric excitations of fractional quantum hall states on quantum computers, *Phys. Rev. Lett.* **129**, 056801 (2022).
- [50] D. X. Nguyen, K. Prabhu, A. C. Balram, and A. Gromov, Supergravity model of the haldane-rezayi fractional quantum hall state, *Phys. Rev. B* **107**, 125119 (2023).
- [51] W. Yuzhu and Y. Bo, Geometric fluctuation of conformal hilbert spaces and multiple graviton modes in fractional quantum hall effect, *Nature Communications* **14**, 2317 (2023).
- [52] F. D. M. Haldane, Fractional quantization of the hall effect: A hierarchy of incompressible quantum fluid states, *Phys. Rev. Lett.* **51**, 605 (1983).
- [53] S. A. Trugman and S. Kivelson, Exact results for the fractional quantum Hall effect with general interactions, *Phys. Rev. B* **31**, 5280 (1985).
- [54] See supplemental material for details, .
- [55] B. Estienne, Z. Papić, N. Regnault, and B. A. Bernevig, Matrix product states for trial quantum hall states, *Phys. Rev. B* **87**, 161112 (2013).
- [56] M. P. Zaletel and R. S. K. Mong, Exact matrix product states for quantum hall wave functions, *Phys. Rev. B* **86**, 245305 (2012).
- [57] V. Crépel, B. Estienne, B. A. Bernevig, P. Lecheminant, and N. Regnault, Matrix product state description of halperin states, *Phys. Rev. B* **97**, 165136 (2018).
- [58] B. A. Bernevig and F. D. M. Haldane, Generalized clustering conditions of jack polynomials at negative jack parameter α , *Phys. Rev. B* **77**, 184502 (2008).
- [59] B. A. Bernevig and F. D. M. Haldane, Model fractional quantum hall states and jack polynomials, *Phys. Rev. Lett.* **100**, 246802 (2008).
- [60] D.-H. Lee and S.-C. Zhang, Collective excitations in the ginzburg-landau theory of the fractional quantum hall effect, *Phys. Rev. Lett.* **66**, 1220 (1991).
- [61] P. Kalinay, P. Markoš, L. Šamaj, and I. Travěnek, The sixth-moment sum rule for the pair correlations of the two-dimensional one-component plasma: Exact result, *Journal of Statistical Physics* **98**, 639 (2000).
- [62] T. Can, M. Laskin, and P. Wiegmann, Fractional quantum hall effect in a curved space: Gravitational anomaly and electromagnetic response, *Phys. Rev. Lett.* **113**, 046803 (2014).
- [63] T. Can, M. Laskin, and P. B. Wiegmann, Geometry of quantum hall states: Gravitational anomaly and transport coefficients, *Annals of Physics* **362**, 752 (2015).

- [64] D. X. Nguyen, T. Can, and A. Gromov, Particle-hole duality in the lowest Landau level, *Phys. Rev. Lett.* **118**, 206602 (2017).
- [65] A. Gromov, S. D. Geraedts, and B. Bradlyn, Investigating anisotropic quantum hall states with bimetric geometry, *Phys. Rev. Lett.* **119**, 146602 (2017).
- [66] J. Wang, S. D. Geraedts, E. H. Rezayi, and F. D. M. Haldane, Lattice monte carlo for quantum hall states on a torus, *Phys. Rev. B* **99**, 125123 (2019).
- [67] P. Kumar and F. D. M. Haldane, A numerical study of bounds in the correlations of fractional quantum Hall states, *SciPost Phys.* **16**, 117 (2024).
- [68] S. Östlund and S. Rommer, Thermodynamic limit of density matrix renormalization, *Phys. Rev. Lett.* **75**, 3537 (1995).
- [69] S. Rommer and S. Östlund, Class of ansatz wave functions for one-dimensional spin systems and their relation to the density matrix renormalization group, *Phys. Rev. B* **55**, 2164 (1997).
- [70] J. Haegeman, J. I. Cirac, T. J. Osborne, I. Pižorn, H. Verschelde, and F. Verstraete, Time-dependent variational principle for quantum lattices, *Phys. Rev. Lett.* **107**, 070601 (2011).
- [71] J. Haegeman, B. Pirvu, D. J. Weir, J. I. Cirac, T. J. Osborne, H. Verschelde, and F. Verstraete, Variational matrix product ansatz for dispersion relations, *Phys. Rev. B* **85**, 100408 (2012).
- [72] Higher energy modes of fractional quantum hall effect, *J. Phys. Through Comput.* **1**, 8 (2018).
- [73] D. Majumder and S. S. Mandal, Neutral collective modes in spin-polarized fractional quantum hall states at filling factors $\frac{1}{3}$, $\frac{2}{5}$, $\frac{3}{7}$, and $\frac{4}{9}$, *Phys. Rev. B* **90**, 155310 (2014).
- [74] B. Yang and F. D. M. Haldane, Nature of quasielectrons and the continuum of neutral bulk excitations in Laughlin quantum hall fluids, *Phys. Rev. Lett.* **112**, 026804 (2014).
- [75] A. C. Balram, G. Sreejith, and J. Jain, Splitting of Girvin-Macdonald-Platzman density wave and the nature of chiral gravitons in fractional quantum hall effect, arXiv preprint arXiv:2406.02730 (2024).
- [76] P. M. Platzman and S. He, Resonant Raman scattering from mobile electrons in the fractional quantum hall regime, *Phys. Rev. B* **49**, 13674 (1994).
- [77] T. D. Rhone, D. Majumder, B. S. Dennis, C. Hirjibehedin, I. Dujovne, J. G. Groshaus, Y. Gallais, J. K. Jain, S. S. Mandal, A. Pinczuk, L. Pfeiffer, and K. West, Higher-energy composite fermion levels in the fractional quantum hall effect, *Phys. Rev. Lett.* **106**, 096803 (2011).
- [78] P. M. Platzman and S. He, Resonant Raman scattering from magneto rotons in the fractional quantum hall liquid, *Physica Scripta* **1996**, 167 (1996).
- [79] K. Park and J. K. Jain, Two-roton bound state in the fractional quantum hall effect, *Phys. Rev. Lett.* **84**, 5576 (2000).
- [80] T. K. Ghosh and G. Baskaran, Modeling two-roton bound state formation in the fractional quantum Hall system, *Phys. Rev. Lett.* **87**, 186803 (2001).
- [81] G. J. Sreejith, A. Wójs, and J. K. Jain, Unpaired composite fermion, topological exciton, and zero mode, *Phys. Rev. Lett.* **107**, 136802 (2011).
- [82] B. Yang, Z.-X. Hu, Z. Papić, and F. D. M. Haldane, Model wave functions for the collective modes and the magnetoroton theory of the fractional quantum hall effect, *Phys. Rev. Lett.* **108**, 256807 (2012).
- [83] C. Repellin, T. Neupert, B. A. Bernevig, and N. Regnault, Projective construction of the F_k Read-Rezayi fractional quantum hall states and their excitations on the torus geometry, *Phys. Rev. B* **92**, 115128 (2015).
- [84] S. Pu, A. C. Balram, M. Fremling, A. Gromov, and Z. Papić, Signatures of supersymmetry in the $\nu = 5/2$ fractional quantum hall effect, *Phys. Rev. Lett.* **130**, 176501 (2023).
- [85] M. Fishman, S. R. White, and E. M. Stoudenmire, The ITensor Software Library for Tensor Network Calculations, *SciPost Phys. Codebases*, 4 (2022).

Supplemental Materials: Resolving Geometric Excitations of Fractional Quantum Hall States

Yang Liu,^{1,2} Tong Zhou Zhao,¹ and T. Xiang^{1,2,*}

¹*Beijing National Laboratory for Condensed Matter Physics and Institute of Physics,
Chinese Academy of Sciences, Beijing 100190, China.*

²*School of Physical Sciences, University of Chinese Academy of Sciences, Beijing 100049, China.*

Appendix A: Parent Hamiltonians of fractional quantum Hall states on a cylinder

In this section, we elucidate the formalism of the fractional quantum Hall effect (FQHE) on a cylinder. While the formalism used in our analysis is conventional, a thorough introduction to these aspects is beneficial, as published articles often omit crucial details. To enhance readability and ensure logical consistency, we will restate some equations previously mentioned in the main text.

The system under consideration is defined on an open cylinder aligned along the x -direction. The length and circumference of the cylinder are denoted as L_x and L_y , respectively. During subsequent infinite tensor network calculations, we take the limit $L_x \rightarrow \infty$. We utilize the Landau gauge $\mathbf{A} = (0, Bx, 0)$ and consider only the orbitals in the lowest Landau level. The m th single-particle wave function in the lowest Landau level is defined as:

$$\phi_m(x, y) = \frac{1}{\sqrt{\pi^{1/2} L_y}} e^{ime_y l y} e^{-(x-me_y l)^2/2} \quad (\text{A1})$$

where $e_y = 2\pi/L_y$ and $l = \sqrt{\hbar c/eB}$ is the magnetic length. In the discussion below, we set below $l = 1$. This Landau orbital has well-defined momentum $k = (k_x, k_y)$ on an infinite cylinder. The momentum along the y -axis is quantized $k_y = me_y$, while that along the x -axis is continuous.

A generic two-body interaction in the momentum space reads

$$v(r_1 - r_2) = \sum_k v_k e^{ik \cdot (r_1 - r_2)}. \quad (\text{A2})$$

By utilizing the formula

$$\langle \phi_{m_1} \phi_{m_2} | e^{ik \cdot (r_1 - r_2)} | \phi_{n_1} \phi_{n_2} \rangle = \langle \phi_{m_1} | e^{ik \cdot r_1} | \phi_{n_1} \rangle \langle \phi_{m_2} | e^{-ik \cdot r_2} | \phi_{n_2} \rangle, \quad (\text{A3})$$

$$\langle \phi_m | e^{ik \cdot r} | \phi_n \rangle = \delta_{(m-n)e_y, k_y} e^{-\frac{k^2}{4} + i\frac{k_x k_y}{2} + ink_x e_y}, \quad (\text{A4})$$

we can further express this two-body interaction, also called the parent Hamiltonian, as

$$H = \sum_{k_x} \sum_m v_k \left(e^{-\frac{1}{4}k^2} \rho_{k_x, me_y} \right) \left(e^{-\frac{1}{4}k^2} \rho_{-k_x, -me_y} \right) = \sum_k V_k \rho_k \rho_{-k} \quad (\text{A5})$$

where ρ_k is the projected density operator

$$\rho_k = \rho_{k_x, me_y} = \sum_n \exp \left[\frac{i\tilde{k}_x(2n+m)}{2} \right] c_n^\dagger c_{n+m}, \quad (\text{A6})$$

$\tilde{k}_x = k_x e_y$, and c_m^\dagger the creation operator of electron. $V_k = [F(k)]^2 v_k$ is the Fourier transform of the projected interaction, and $F(k) = \exp(-k^2/4)$ is the form factor for the lowest Landau level.

The Fourier transform of the V_1 -Haldane pseudopotential or Trugman-Kivelson real space potential $\nabla_i^2 \delta^2(r_i - r_j)$ is $v_k = 1 - k^2$ [1, 2]. It corresponds to the zero energy Laughlin state. Substituting this expression into Eq. (A5), we find the parent Hamiltonian of the Laughlin state to be:

$$H_L = \frac{(2\pi)^{5/2}}{L_y^3} \sum_{j_1 j_2 j_3 j_4} (j_1 - j_2) (j_3 - j_4) e^{-e_y^2 [(j_1 - j_4)^2 + (j_2 - j_3)^2]/2} \delta_{j_1 + j_2, j_3 + j_4} c_{j_1}^\dagger c_{j_2}^\dagger c_{j_3} c_{j_4} \quad (\text{A7})$$

* txiang@iphy.ac.cn

The three-body Hamiltonian for the Moore-Read (MR) state can be similarly derived. The result is

$$H_{\text{MR}} = \sum_{k_1, k_2} V_{k_1, k_2} \rho_{k_1} \rho_{k_2} \rho_{-k_1 - k_2}, \quad (\text{A8})$$

where

$$V_{k_1, k_2} = F(k_1)F(k_2)F(-k_1 - k_2)v(k_1, k_1), \quad (\text{A9})$$

and $v(k_1, k_1)$ is the Fourier transform of the three-body interaction

$$\nabla_i^4 \nabla_j^2 \delta^2(r_i - r_j) \delta^2(r_j - r_k), \quad (\text{A10})$$

which reads

$$v(k_1, k_1) = k_1^4 k_2^2 + k_1^2 k_2^4 + k_2^4 (k_1 + k_2)^2 + k_2^2 (k_1 + k_2)^4 + k_1^4 (k_1 + k_2)^2 + k_1^2 (k_1 + k_2)^4. \quad (\text{A11})$$

H_{MR} can also be expressed as [3, 4]

$$H_{\text{MR}} = \frac{1024\sqrt{3}\pi^7}{L_y^8} \sum_{j_1, j_2, j_3, j_4, j_5, j_6} (j_1 - j_2)(j_1 - j_3)(j_2 - j_3)(j_6 - j_4)(j_6 - j_5)(j_5 - j_4) \delta_{j_1 + j_2 + j_3, j_4 + j_5 + j_6} \exp \left\{ -\frac{2\pi^2}{L_y^2} \left[\sum_i j_i^2 - \frac{1}{6} \left(\sum_i j_i \right)^2 \right] \right\} c_{j_1}^\dagger c_{j_2}^\dagger c_{j_3}^\dagger c_{j_4} c_{j_5} c_{j_6} \quad (\text{A12})$$

Appendix B: MPS representation of the ground state

For a translation invariant system, the MPS of the ground state reads

$$\Psi = \dots \text{---} \textcircled{A} \text{---} \textcircled{A} \text{---} \textcircled{A} \text{---} \dots, \quad (\text{B1})$$

where A is the local tensor defined for a unit cell. If this unit cell contains M sites, we further decompose A as a product of M local tensors defined on each site by $A_l (l = 1, \dots, M)$.

The Laughlin ground states are three-fold topological degenerate, corresponding to the following three initial orbital configurations (or the root partitions [5–7]): $\{\dots 100100\dots\}$, $\{\dots 010010\dots\}$, and $\{\dots 001001\dots\}$. Thus, we can set $M = 3$ and represent A as

$$\text{---} \textcircled{A} \text{---} = \text{---} \textcircled{A_1} \text{---} \textcircled{A_2} \text{---} \textcircled{A_3} \text{---} \quad (\text{B2})$$

The Laughlin state conserves the particle number and the y -axis momentum on a cylinder [8, 9]. Thus, we can assign both the particle number C_l and the momentum K_l to the vertical leg of local tensor A_l . For a given filling factor ν , (K_l, C_l) are defined by [8–10]

$$K_l = l(N_l - \nu), \quad (\text{Momentum}) \quad (\text{B3})$$

$$C_l = N_l - \nu, \quad (\text{Particle number}) \quad (\text{B4})$$

where N_l is the particle number at site l . Similarly, we can introduce the corresponding quantum numbers $(\overline{K}, \overline{C})$ for each horizontal bond.

Under a translation by M sites, the physical and virtual momenta, K_l and \overline{K}_l , behave as

$$K_l \rightarrow K_l + MC_l, \quad (\text{B5})$$

$$\overline{K}_l \rightarrow \overline{K}_l + M\overline{C}_l. \quad (\text{B6})$$

This property should be taken into account in the implementation of the DMRG algorithm [9, 11, 12] and in the translation of MPS with a periodicity M .

For each local tensor, the quantum numbers satisfy the following addition rule:

$$(\bar{K}, \bar{C})_{l,\text{left}} + (K_l, C_l) - (\bar{K}, \bar{C})_{l,\text{right}} = 0 \quad (\text{B7})$$

A similar idea works for the Moore-Read (MR) state. In the even parity state, we can choose the orbital configuration $\{\dots 10011001\dots\}$ to represent the ground state. This indicates that the minimum cell of the ground state is $M = 4$ and

$$\text{---} \bigcirc_A \text{---} = \text{---} \bigcirc_{A_1} \text{---} \bigcirc_{A_2} \text{---} \bigcirc_{A_3} \text{---} \bigcirc_{A_4} \text{---} \cdot \quad (\text{B8})$$

In the odd-parity sector of the MR state, there are unpaired fermions. In this case, the initial orbital configuration changes from $\{\dots 1001\dots\}$ to $\{\dots 01\dots\}$, and the corresponding unit cell changes from 4 to 2. Thus, A can be represented as

$$\text{---} \bigcirc_A \text{---} = \text{---} \bigcirc_{A_1} \text{---} \bigcirc_{A_2} \text{---} \cdot \quad (\text{B9})$$

In addition, a one-half quantum flux $f = 1/2$ should attach to a local tensor in each unit cell to correctly capture the topological nature of the neutral fermion mode. Accordingly, Eq. (B7) becomes

$$(\bar{K}, \bar{C})_{l,\text{left}} + (K_l + f, C_l) - (\bar{K}, \bar{C})_{l,\text{right}} = (0, 0) \quad (\text{B10})$$

We determine all local tensors by variationally minimizing the ground state energy using the standard tensor-network methods, including the density matrix renormalization group (DMRG) and variational uniform matrix product states (VUMPS) [13]. For benchmarking, we calculate the entanglement spectrum of both the Laughlin and MR states. As shown in Fig. 1, the entanglement spectrum patterns of these two states obtained from our calculation are consistent with the CFT.

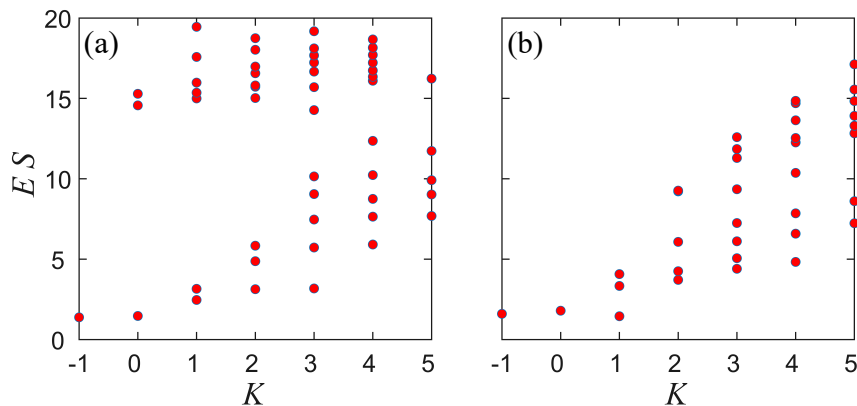


FIG. 1. Entanglement spectra of (a) the Laughlin state, the counting pattern is 1,1,2,3,5,..., and (b) the MR state, the counting pattern is 1,1,3,5,... [14].

Appendix C: MPS representation of excited states under the single-mode approximation

Under the single-mode approximation, the excited states are represented by replacing one of the A tensors in the ground state with an impurity tensor B and then boosting into a momentum eigenstate

$$\Phi_k(B) = \sum_n e^{i\tilde{k}_x n M} \dots \text{---} \bigcirc_{A}^{n-1} \text{---} \bigcirc_B^n \text{---} \bigcirc_A^{n+1} \text{---} \dots \cdot \quad (\text{C1})$$

In this expression, B is defined on one of the unit cells. Like A , it can be further decomposed as sum of M MPS

$$\text{---} \bigcirc_B \text{---} = \text{---} \bigcirc_{B_1} \text{---} \bigcirc_{A_2} \text{---} \dots \text{---} \bigcirc_{A_M} \text{---} + \dots + e^{i\tilde{k}_x (M-1)} \text{---} \bigcirc_{A_1} \text{---} \bigcirc_{A_2} \text{---} \dots \text{---} \bigcirc_{B_M} \text{---} \cdot, \quad (\text{C2})$$

where $\tilde{k}_x = e_y k_x$ and (B_1, \dots, B_M) are the local impurity tensors to be variationally determined. In the study of neutral fermions in the odd-parity sector of the MR state, as the unit cell is reduced from $M = 4$ to 2, we should shift the central momentum from 0 to π , by setting $\tilde{k}_x \rightarrow \tilde{k}_x \pm \frac{\pi}{2}$.

It is simple to show that the above MPS is invariant under the following gauge transformation

$$B_l \rightarrow B_l + A_l X_l - e^{-ik} X_l A_l, \quad (\text{C3})$$

where X_l is an arbitrary bond matrix.

Clearly, $\Phi_k(B)$ is orthogonal to the ground state, $\langle \Psi(A) | \Phi_k(B) \rangle = 0$, if k is finite. To ensure $\Phi_k(B)$ orthogonal to the ground state even in the case $k = 0$, B_l should also be orthogonal to A_l if (A_1, \dots, A_M) are left canonicalized, satisfying the constraint



$$= 0. \quad (\text{C4})$$

In this case, B_l can be further parameterized as



$$= \quad (\text{C5})$$

where V_l is the null-space tensor of A_l and X_l is variational bond matrix determined by the equation [15]

$$H_k^{\text{eff}} X = E_k X, \quad (\text{C6})$$

where H_k^{eff} is the effective Hamiltonian determined by the derivative

$$H_k^{\text{eff}} = \frac{\delta^2}{\delta(X')^\dagger \delta X} \langle \Phi_k(B') | H | \Phi_k(B) \rangle, \quad (\text{C7})$$

where $X = (X_1, \dots, X_M)$.

For details on the evaluation of the effective Hamiltonian H^{eff} , we refer readers to Ref. [16].

Appendix D: Static structure factor

In Fig. 1 of the main text, we show the static structure factor $S(k)$ along the k_x direction with $k_y = 0$. Here, we provide more information on this static structure factor for the Laughlin and MR states. Figure 2 shows the density plot of $S(k)$ on the whole (k_x, k_y) plane. Our calculation indicates that $S(k)$ is isotropic. The peak (high intensity) positions of $S(k)$ are consistent with previous studies [17].

-
- [1] F. D. M. Haldane, Fractional quantization of the hall effect: A hierarchy of incompressible quantum fluid states, *Phys. Rev. Lett.* **51**, 605 (1983).
 - [2] S. A. Trugman and S. Kivelson, Exact results for the fractional quantum Hall effect with general interactions, *Phys. Rev. B* **31**, 5280 (1985).
 - [3] A. Kirmani, K. Bull, C.-Y. Hou, V. Saravanan, S. M. Saeed, Z. Papić, A. Rahmani, and P. Ghaemi, Probing geometric excitations of fractional quantum hall states on quantum computers, *Phys. Rev. Lett.* **129**, 056801 (2022).
 - [4] C. Voinea, S. Pu, A. Kirmani, P. Ghaemi, A. Rahmani, and Z. Papić, Deformed fredkin model for the $\nu = 5/2$ moore-read state on thin cylinders, *Phys. Rev. Res.* **6**, 013105 (2024).
 - [5] B. A. Bernevig and F. D. M. Haldane, Generalized clustering conditions of jack polynomials at negative jack parameter α , *Phys. Rev. B* **77**, 184502 (2008).
 - [6] B. A. Bernevig and F. D. M. Haldane, Model fractional quantum hall states and jack polynomials, *Phys. Rev. Lett.* **100**, 246802 (2008).
 - [7] B. Yang, Z.-X. Hu, Z. Papić, and F. D. M. Haldane, Model wave functions for the collective modes and the magnetoroton theory of the fractional quantum hall effect, *Phys. Rev. Lett.* **108**, 256807 (2012).
 - [8] M. P. Zaletel and R. S. K. Mong, Exact matrix product states for quantum hall wave functions, *Phys. Rev. B* **86**, 245305 (2012).

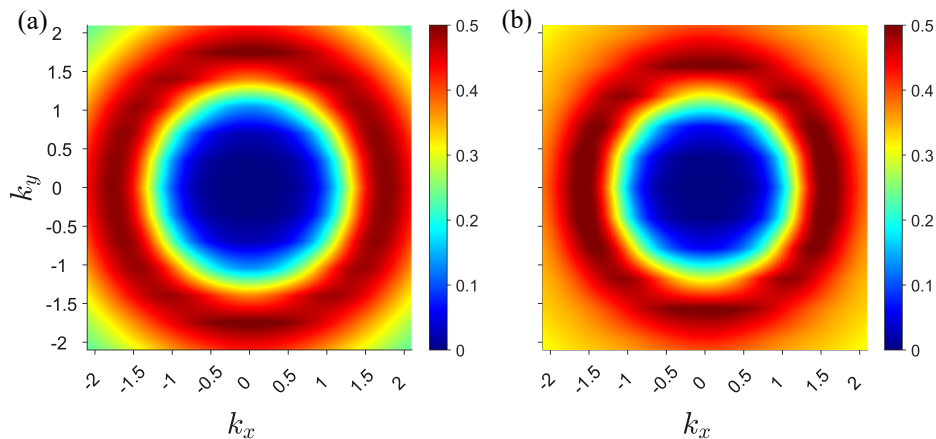


FIG. 2. Density plot of the static structure factor $S(k)$ defined in Eq. (7) of the main text in the (k_x, k_y) plane for (a) the Laughlin state with $L_y = 18$ and (b) the MR state with $L_y = 16$.

- [9] M. P. Zaletel, R. S. K. Mong, and F. Pollmann, Topological characterization of fractional quantum hall ground states from microscopic hamiltonians, *Phys. Rev. Lett.* **110**, 236801 (2013).
- [10] L. Hu and W. Zhu, Abelian origin of $\nu = 2/3$ and $2 + 2/3$ fractional quantum hall effect, *Phys. Rev. B* **105**, 165145 (2022).
- [11] S. R. White, Density matrix formulation for quantum renormalization groups, *Phys. Rev. Lett.* **69**, 2863 (1992).
- [12] S. R. White, Density-matrix algorithms for quantum renormalization groups, *Phys. Rev. B* **48**, 10345 (1993).
- [13] V. Zauner-Stauber, L. Vanderstraeten, M. T. Fishman, F. Verstraete, and J. Haegeman, Variational optimization algorithms for uniform matrix product states, *Phys. Rev. B* **97**, 045145 (2018).
- [14] H. Li and F. D. M. Haldane, Entanglement spectrum as a generalization of entanglement entropy: Identification of topological order in non-abelian fractional quantum hall effect states, *Phys. Rev. Lett.* **101**, 010504 (2008).
- [15] L. Vanderstraeten, J. Haegeman, and F. Verstraete, Tangent-space methods for uniform matrix product states, *SciPost Phys. Lect. Notes*, **7** (2019).
- [16] T. Xiang, *Density matrix and tensor network renormalization* (Cambridge University Press, 2023).
- [17] J. Wang, S. D. Geraedts, E. H. Rezayi, and F. D. M. Haldane, Lattice monte carlo for quantum hall states on a torus, *Phys. Rev. B* **99**, 125123 (2019).